

dune ridges and the modern prevailing winds and between the directions of present and past sand movement suggest that the sand sea may have formed in a wind regime similar to the modern regime, in which a major component is a strong ENE wind.

Recognition of the large dunes allows reinterpretation of linear and curvilinear trends identified previously in Landsat summer scenes of the sand sea area and ascribed to bedrock structural control (4, 13). The trends reported were a NE-SW to ENE-WSW linear trend, a nearly orthogonal NW-SE linear trend, and elliptical or crescentic trends and were identified on the basis of lake alignments, lake shape, and lake-free areas and by means of a texture analyzer. The trends are reinterpreted here in terms of the morphology of the sand sea and the subsequent development of thermokarst lakes. The NE-SW to ENE-WSW trends are determined by dune ridges and chains of thermokarst lakes in interdune troughs, the elliptical or crescentic trends occur where chains of lakes enclose dune ridges or the nose of a ridge, and the NW-SE trends are a result of lake elongation perpendicular to the prevailing winds.

This stabilized sand sea is the most extensive field of large dunes yet reported in the North American Arctic. At the sand sea's eastern edge, eolian sand overlies Quaternary alluvial and marine deposits; at its southern edge, 20 m of eolian sand overlies at least 15 m of alluvial sand and silt. East of Teshekpuk Lake, the linear northern margin of the large dunes is oblique to the dominant ridge trend. Because marine deposits are common at or near the surface to the north, this boundary may be an ancient shoreline.

The age of inception and periods of activity of the sand sea are uncertain, but Late Wisconsinan seems the most reasonable age assignment for the latest episode of activity. Further study of the eolian sand and the adjacent and subjacent deposits should provide more precise dating, will improve our understanding of Pleistocene paleoclimate and paleoecology of the Arctic Coastal Plain, and will yield additional information on the distinctive sedimentary structures of eolian deposits formed in cold climates (14). Knowledge of the history of eolian activity is desirable for an assessment of the sensitivity of the environment to human activity in the National Petroleum Reserve in Alaska.

L. DAVID CARTER

U.S. Geological Survey,
Menlo Park, California 94025

References and Notes

1. E. D. McKee, *U.S. Geol. Surv. Prof. Pap. 1052* (1979), pp. 1 and 82.
2. R. F. Black, *Arctic* 4, 89 (1951).
3. L. W. Gatto and D. M. Anderson, *Science* 188, 255 (1975).
4. W. A. Fischer and E. H. Lathram, *Oil Gas J.* 71, 97 (1973); E. H. Lathram, I. L. Tailleux, W. W. Patton, Jr., W. A. Fischer, in *Symposium on Significant Results Obtained from Earth Resources Technology Satellite 1*, vol. 2, *Summary of Results*, S. C. Freden, E. P. Mercanti, D. E. Witten, Eds. (NASA, Greenbelt, Md., 1973), p. 31.
5. R. F. Black, *U.S. Geol. Surv. Prof. Pap. 302-C* (1964), p. 59; J. B. O'Sullivan, thesis, Iowa State University of Science and Technology, Ames (1961).
6. Refer to the U.S. Geological Survey 1:63,360 series topographic maps of the following quadrangles: Teshekpuk (A-1) through (A-3) and (B-1) through (B-3); Harrison Bay (A-5) and (B-3) through (B-5); and Umiat (D-4) and (D-5). See also the U.S. Geological Survey 1:250,000 series topographic map of the Ikpikuk River quadrangle.
7. Identified by C. R. Repenning (personal communication).
8. A. V. Sher, *Int. Geol. Rev.* 16, 1 (1974).
9. L. D. Carter and S. W. Robinson, *U.S. Geol. Surv. Open-File Rep. 78-320* (1978); *American Quaternary Association Abstracts of the Fifth Biennial Meeting* (1978), p. 192.
10. P. V. Sellmann, J. Brown, R. I. Lewellen, H. McKim, C. Merry, *U.S. Army Corps Eng. Cold Reg. Res. Eng. Lab. Res. Rep. 344* (1975).
11. C. E. Carson and K. M. Hussey, *J. Geol.* 70, 417 (1962).
12. S. G. Fryberger, *U.S. Geol. Surv. Prof. Pap. 1052* (1979), p. 137.
13. A. F. Maurin and E. H. Lathram, *U.S. Geol. Surv. Prof. Pap. 1015* (1977), p. 213.
14. T. S. Ahlbrandt and S. Andrews, *Palaeogeogr. Palaeoclimatol. Palaeoecol.* 25, 327 (1978).
15. I thank L. W. Gatto for supplying the Landsat image used in this report and P. V. Sellmann for permitting reproduction of the lake elongation data. I also thank D. M. Hopkins and J. R. Williams for reviewing the manuscript and J. P. Galloway and M. P. Springer for assisting in the field.

21 July 1980; revised 4 November 1980

Noble Gases in Stratospheric Dust Particles: Confirmation of Extraterrestrial Origin

Abstract. *Noble gas elemental and isotopic ratios were measured in a group of 13 "chondritic" stratospheric dust particles. Neon and argon are present in "solar" proportions; xenon appears to be dominated by contributions from "planetary" sources. The apparent xenon concentration is higher than that measured in any bulk meteorite, approaching the concentration found in the noble gas-rich, acid-insoluble residues from carbonaceous chondrites.*

"Chondritic" dust particles, collected in the stratosphere by high-flying (20 km) National Aeronautics and Space Administration U-2 aircraft, represent a new class of solar system material now available for study (1). Evidence that some of these particles may be of extraterrestrial origin has come from a variety of approaches. These include observations of high helium concentrations suggestive of solar wind exposure (2) and trace element abundances consistent with those of primitive meteorites and distinctly different from those of terrestrial crustal rocks (3, 4). We report here rare gas elemental and isotopic data which confirm the extraterrestrial nature of these particles and provide some additional insight into their history.

Because of the small mass of individual particles ($\sim 10^{-9}$ g), we selected 13 "chondritic" aggregates (5) from a collector supplied by D. Brownlee and analyzed the noble gases released in a single extraction from the entire group. Differences in the size, morphology, and chemistry of the individual particles (Table 1) may reflect fundamental differences between the particles (6) or differences in heating upon atmospheric entry, or both. In addition, each particle may have a unique preatmospheric history. All of these factors are likely to contribute to variations in the noble gases among the individual particles.

The total mass of the particles is estimated to be $\sim 10^{-8}$ g, and the total cross-sectional area is $\sim 10^{-5}$ cm².

Neon, argon, krypton, and xenon were analyzed statically in an ion-counting mass spectrometer coupled to a low-blank, gas-handling system (7). We extracted the gases in stepwise heatings of 1400°, 1500°, and 1600°C by dropping a nickel "boat" containing the particles into an extensively degassed tungsten coil. Each temperature step was maintained for 15 minutes with the first step, during which apparently most of the gas was extracted, chosen to be below the melting point of nickel (1453°C). The evolved gases were purified by exposure to freshly deposited titanium films (in three stages) and separated by selective adsorption on activated charcoal for individual analyses. Details of the gas handling and the mass spectroscopy are similar to those reported by Bernatowicz *et al.* (8) except that all gases were measured in the ion-counting mode. Isotopic spectra were obtained by programmed peak-jumping with a cumulative counting time at each isotope of 500 seconds. Prior to analysis, the tungsten coil was fluxed with nickel foil and extensively outgassed (100 hours at 2000°C), and the gas-handling system was maintained at a temperature in excess of 100°C for about a week. This treatment reduced the 1400°C system procedural blanks to ap-

proximately 2×10^8 , 10^7 , 10^5 , and 10^4 atoms of ^{20}Ne , ^{36}Ar , ^{84}Kr , and ^{132}Xe , respectively.

The noble gas abundances measured in the final sequence of procedural blanks (both bare coil and nickel foil blanks) and from the stratospheric dust sample are listed in Table 2 where the signals are given directly in counts per second, uncorrected for any extraneous contributions. The observed neon, krypton, and xenon 1400°C blanks were constant to approximately 25 percent, and

the neon and xenon abundances from the 1400°C extraction of the particles were significantly above blank levels (by factors of 1.7 and 3.0, respectively). Data obtained from the 1500° and 1600°C extractions were indistinguishable from the respective blanks. For krypton, the signal was at blank level so that the observed signal establishes only an upper limit. The argon blanks were quite variable, possibly a result of argon introduced in the manufacture of the tungsten heating coil and released when the

coil was alloyed with nickel foil. However, the argon measured in the particles shows a significant isotopic enrichment of ^{36}Ar and ^{38}Ar relative to ^{40}Ar with respect to terrestrial argon (Figs. 1 and 2). Virtually all of the signal at mass 37 is due to $^{37}\text{Cl}^+$. The chlorine component also contributes small signals at masses 36 and 38 due to $^1\text{H}^{35}\text{Cl}^+$ and $^1\text{H}^{37}\text{Cl}^+$. The HCl^+/Cl^+ ratio is observed to be constant ($\text{HCl}^+/\text{Cl}^+ = 0.012 \pm 0.006$), probably due to the fact that $\text{H}/\text{Cl} \gg 1$ in the mass spectrometer (7). Argon from the terrestrial atmosphere contributes at masses 36, 38, and 40 ($^{40}\text{Ar}/^{36}\text{Ar} = 295.5$, $^{38}\text{Ar}/^{36}\text{Ar} = 0.187$). In addition there are small signals at all masses presumably due to organic contamination ($37/36 \sim 38/36 \sim 39/36 \sim 40/36 \sim 1$). The blank runs plotted in Figs. 1 and 2 show mixtures of air and the $\text{HCl}-\text{Cl}$ component, as an approximately linear array between the two end-members, but with small amounts of the organic component displacing the points below the line in Fig. 1 and above the line in Fig. 2. In the case of the sample, however, displacement from the mixing line in Fig. 1 is best explained in terms of the addition of solar wind argon ($^{40}\text{Ar}/^{36}\text{Ar} \sim 0$, $^{38}\text{Ar}/^{36}\text{Ar} = 0.187$). Although the organic contamination is in the same direction as solar wind in Fig. 1, it would require approximately a tenfold increase in the organic component over the average 1400°C blank and there is no large concomitant displacement in Fig. 2. Alternatively, the deviation could be due to variations in the chlorine background, but this alternative would require an eightfold increase in the HCl^+/Cl^+ ratio which seems unlikely. In addition, in Fig. 2, where air and solar wind argon are indistinguishable, there is no deviation from the approximate mixing line established by the blank measurements; thus the component that causes the deviation in Fig. 1 must have a 36/38 ratio similar to that of terrestrial or solar wind argon (~ 5.3) as opposed to the HCl/Cl component with $36/38 \sim 3$ or the organic component with $36/38 \sim 1$.

In these paragraphs we summarize the blank-corrected data, where errors (1σ , where σ is the standard deviation) have been assigned on the basis of observed variations in the blanks and the statistical errors in the measurements only. The observed concentration of ^{20}Ne is $4.4 \pm 1.6 \times 10^{-4}$ cubic centimeter at standard temperature and pressure (STP) per gram, roughly 4 percent of the value of 1.2×10^{-2} measured in the 1.4- μm fraction of lunar soil 10084 (9) and roughly five times the concentration observed in the gas-rich meteorite Pe-

Table 1. Characteristics of the particles analyzed; SPH is an estimate of particle sphericity (the surface area of a sphere of equal volume divided by the particle surface area) to indicate the reentrant character of the particle structure (5). The elemental ratios (atomic) were obtained as a result of a comparison of the energy-dispersive x-ray peak ratios to the peak ratios measured on a powdered standard from the Allende meteorite (4). Particle geometry effects may contribute significantly to variations between particles, especially for iron and nickel. Averages are particle averages, not volume- or area-weighted averages. The averages from (20) were obtained on a different set of particles and with the use of more quantitative methods.

Particle designation	Diameter (μm)	SPH	Elemental abundances relative to Si					
			Mg	Al	S	Ca	Fe	Ni
18-2-02	7.3	0.4	0.76	0.20	0.35	0.08	0.48	0.03
18-2-06	8.3	0.2	0.81	0.20	0.50	0.04	0.53	0.03
18-2-07	8.7	0.6	0.76	< 0.01	0.47	0.07	0.35	0.03
18-3-01	11.4	0.2	0.62	0.18	0.23	0.05	0.52	0.06
18-3-02	14.2	0.1	0.81	0.13	0.25	0.03	0.44	0.03
18-3-07	15.5	0.2	0.67	0.10	0.57	0.02	0.51	0.06
18-4-01B	10.5	0.4	0.91	0.15	0.14	0.04	0.41	0.04
18-4-04	8.3	0.1	1.15	0.13	0.08	0.02	0.15	0.01
18-4-11	9.9	0.2	1.20	0.05	0.07	0.01	0.38	0.01
18-5-03	7.8	0.6	0.53	0.20	0.14	0.03	0.59	0.02
18-5-08	6.9	0.2	1.10	0.13	0.04	0.05	0.16	< 0.01
18-5-17B	13.2	0.2	1.05	0.10	< 0.01	0.03	0.33	0.03
18-5-20	19.8	0.3	0.24	< 0.01	< 0.01	0.01	0.60	0.03
Average	10.9	0.3	0.81	0.13	0.22	0.04	0.42	0.03
Average [given in (20)]			0.85	0.06	0.35	0.05	0.63	0.04

Table 2. Noble gas results. Data in parentheses have been corrected for various interferences; NA, not measured. The ^{20}Ne signal has been corrected for $^{40}\text{Ar}^{2+}$, as monitored in terms of the $^{40}\text{Ar}^+$ present during the run, based on the ratio $^{40}\text{Ar}^{2+}/^{40}\text{Ar}^+ = 0.087$ (7); ^{36}Ar and ^{38}Ar have been corrected for HCl^+ ($\text{HCl}^+/\text{Cl}^+ = 0.012$) as monitored by signals at masses 35 and 37. The ^{36}Ar and ^{38}Ar have also been corrected for atmospheric contributions on the basis of the measured ^{40}Ar since it is clear that very little of the measured ^{40}Ar can arise from the decay of ^{40}K in the particles. An upper limit for the potassium content, obtained from the absence of detectable signals in energy-dispersive x-ray analysis at the 0.5 percent level, implies an upper limit of about 3×10^{-12} cm 3 STP of radiogenic ^{40}Ar , if we assume a 4.6×10^9 year accumulation time, much less than the observed signal at mass 40 (1.9×10^{-10} cm 3 STP). No corrections have been made to the krypton or xenon data.

Description	Run No.	Observed signal at various masses (count/sec)						
		20	36	37	38	40	84	132
Average spectrometer blank		3 (3)	15 (0)	369	8 (4)	10	0.1	0.1
1400°C blank	44	285 (262)	27 (3)	229	12 (6)	4,400	1.1	0.4
1400°C, 18 mg Ni	46	206 (185)	37 (1)	258	14 (6)	7,500	0.6	0.6
1400°C blank	48	281 (258)	152 (9)	410	41 (12)	37,000	1.0	0.6
1400°C blank	50	222 (198)	49 (8)	328	16 (7)	8,200	NA	NA
1400°C, 18 mg Ni	54	162 (142)	NA	NA	NA	NA	0.7	0.5
Average, 1400°C blank		231 (209)	(5)	306	(7)		0.9	0.5
1500°C blank	49	503 (476)	276 (21)	432	67 (18)	70,000	2.0	1.5
1600°C blank	45	732 (699)	180 (10)	447	42 (8)	46,000	2.3	0.6
1600°C, 18 mg Ni	47	954 (928)	504 (-14)	410	108 (9)	148,000	2.8	0.9
Sample, 1400°C	51	380 (355)	215 (87)	405	49 (23)	33,000	0.8	2.0
Sample, 1500°C	52	284 (260)	232 (27)	378	56 (15)	50,000	1.6	0.2
Sample, 1600°C	53	821 (797)	669 (46)	397	138 (20)	179,000	5.1	0.6

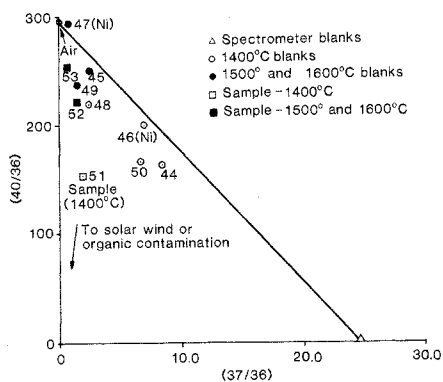


Fig. 1. Three-isotope graph of the signals at masses 40 and 37 divided by the signals at mass 36. The sample measurement shows a large enrichment in the signal at mass 36 relative to the signals at masses 40 and 37. Comparisons with Fig. 2 show that this effect cannot be due to admixture with either hydrocarbons (36:38:40 ~ 1:1:1) or a chlorine-derived component (36:38:40 ~ 3:1:0).

syanoes (10). The $^{20}\text{Ne}/^{36}\text{Ar}$ ratio in the particles is 9 ± 3 , similar to the ratio of 7.1 obtained from the 1.4- μm fraction of lunar sample 10084 (8) and the value of 15 found in Pesyanoe (10) but quite distinct from the planetary (or terrestrial) value of ~ 0.5 . The $^{21}\text{Ne}/^{22}\text{Ne}$ ratio is 0.03 ± 0.01 . The $^{20}\text{Ne}/^{22}\text{Ne}$ ratio of 11 ± 3 is compatible with either solar or planetary sources. The abundances of ^{36}Ar ($5.1 \pm 0.3 \times 10^{-13}$ cm 3 STP) and ^{38}Ar are substantially above blank level with $^{36}\text{Ar}/^{38}\text{Ar}$ approximately 5, in agreement with all known (noncosmogenic) solar system sources. An upper limit of 4×10^{-15} cm 3 STP is obtained for ^{84}Kr . The abundance of ^{132}Xe ($\sim 10^{-15}$ cm 3 STP) is above the average 1400°C blank by a factor of 3, and the signal at mass 132 in the 1400°C extraction was larger by an order of magnitude than that observed in the 1500°C extraction (which included any gases liberated by the melting nickel foil). We therefore have some degree of confidence that the xenon data represent a measure of the gas indigenous to the sample.

Figure 3 compares noble gas elemental abundances in these particles with those of other solar system reservoirs. The lighter gases are distributed with a solar-like pattern, characteristic of that observed in the lunar soil and gas-rich meteorites and distinctly different from that characteristic of the terrestrial atmosphere and trapped noble gases in carbonaceous chondrites, usually referred to as planetary. In view of current estimates of the solar wind flux (11), the solar wind exposure time required at 1 AU to accumulate the observed neon and argon is of the order of 15 to 45 years if we assume the absence of saturation effects.

Since the $^{21}\text{Ne}/^{20}\text{Ne}$ ratio is solar with no obvious cosmogenic ^{21}Ne , an upper limit for the cosmic-ray exposure age of 130×10^6 years can be set if we assume the upper error extremity and a production rate of 4×10^{-9} cm 3 of ^{21}Ne per gram per 10^8 years (12).

The ^{132}Xe concentration of $\sim 10^{-7}$ cm 3 STP per gram and the elemental pattern shown in Fig. 3 suggests a substantial contribution from planetary sources. The $^{132}\text{Xe}/^{20}\text{Ne}$ ratio observed in the particles is 2.3×10^{-4} , compared with a value for bulk lunar soil (1.4- μm fraction) of 1.8×10^{-5} (9) and the (planetary) value of about 2×10^{-2} observed in the Murray and Renazzo meteorites (13). The corresponding value for the terrestrial atmosphere is 1.6×10^{-3} . It is unlikely that the heavy noble gas abundance pattern can be explained as representing a mixture of terrestrial and solar gases since the upper limit for the $^{84}\text{Xe}/^{132}\text{Xe}$ ratio of 4 is less than either the solar value of about 10 (14) or the terrestrial value of 27.8. The observed isotopic composition of xenon is as follows: $^{128}\text{Xe}/^{132}\text{Xe} = 0.1 \pm 0.1$, $^{129}\text{Xe}/^{132}\text{Xe} = 1.0 \pm 0.1$, $^{130}\text{Xe}/^{132}\text{Xe} = 0.1 \pm 0.1$, $^{131}\text{Xe}/^{132}\text{Xe} = 0.9 \pm 0.2$, $^{134}\text{Xe}/^{132}\text{Xe} = 0.4 \pm 0.1$, and $^{136}\text{Xe}/^{132}\text{Xe} = 0.3 \pm 0.1$. This isotopic structure, as uncertain as it is, suggests the absence of any drastically large isotopic anomalies, but it is not sufficiently precise to resolve isotopically the difference between solar, terrestrial, or planetary sources. If the xenon measurement is correct, the concentration is considerably higher than that found in bulk meteorites [for example, Murray, with one of the highest planetary xenon concentrations (15), contains only 1×10^{-8}

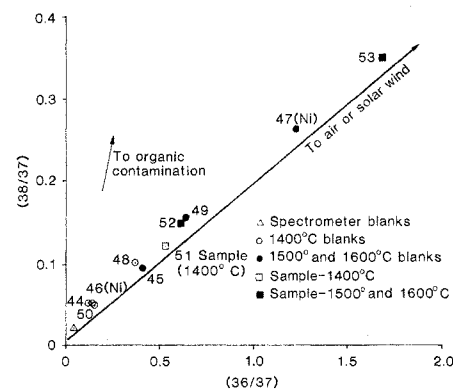


Fig. 2. Three-isotope graph of the signals at masses 36 and 38 divided by the signal mass 37. Procedural blanks define an approximate mixing line between the spectrometer blank and atmospheric argon. The sample measurement shows no significant enrichments in the signal at mass 38 relative to the signals at masses 36 and 37, an indication that the enrichments in mass 36 seen in Fig. 1 are most likely due to solar wind argon (see text).

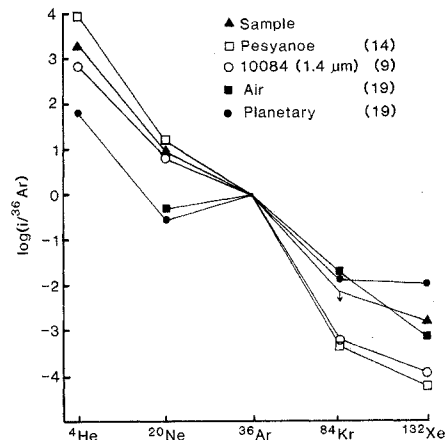


Fig. 3. Noble gas abundance pattern, normalized to ^{36}Ar , for the stratospheric dust sample. Planetary gas (carbonaceous chondrites and terrestrial atmosphere) and solar gas (lunar soil 10084 and the gas-rich meteorite Pesyanoe) are shown for comparison. The ^4He content was measured by Rajan *et al.* (2) on a different set of particles.

cm 3 STP of ^{132}Xe per gram]. The implied xenon concentration in the particles approaches that found in the planetary gas-rich acid residues of carbonaceous chondrites, for example, 3×10^{-7} cm 3 STP of ^{132}Xe per gram in the 3C1 Allende residue (16).

Even though the elemental and isotopic structure of the noble gases indicates an extraterrestrial origin, the earth's upper atmosphere is a potential source for noble gases that should not be overlooked. Because of the high (> 10 km/sec) velocity of incidence, the process of deceleration is a mechanism for low-energy implantation of upper atmospheric gases. Above 400 km, strong fractionation effects dominate the elemental and isotopic composition of the atmosphere (17), which might, in principle, provide the observed anomalies. Other data indicate, however, that atmospheric mixing preserves the sea-level isotopic composition at altitudes below about 200 km, and in the region where most of the deceleration occurs (~ 90 km) atmospheric isotopic ratios are demonstrably terrestrial (18). Moreover, it is difficult to generate the observed elemental pattern as well as the nonterrestrial $^{40}\text{Ar}/^{36}\text{Ar}$ by any such fractionation and still preserve a normal $^{36}\text{Ar}/^{38}\text{Ar}$ ratio of ~ 5 . Even so, in the worst case, if a particle sweeps out and retains twice its mass in upper atmospheric gases, it still falls short by a factor of 2 of implanting the observed quantity of neon. Such an efficient implantation could, of course, not exist in reality since the resulting unlikely particle would have increased in mass by a factor of 3 and be nearly pure nitrogen. In summary, elemental and isotopic abundance

data suggest that the noble gases are indeed of extraterrestrial origin and represent a mixture of solar and planetary components.

B. HUDSON, G. J. FLYNN
P. FRAUNDORF, C. M. HOHENBERG
J. SHIRCK*

McDonnell Center for the Space
Sciences, Washington University,
St. Louis, Missouri 63130

References and Notes

1. D. E. Brownlee, *NASA Tech. Memo. X-73* (1976).
2. R. S. Rajan, D. E. Brownlee, D. Tomandl, P. W. Hodge, H. Farrar, R. A. Britten, *Nature (London)* **267**, 133 (1977).
3. R. Ganapathy and D. E. Brownlee, *Science* **206**, 1075 (1979).
4. G. J. Flynn, P. Fraundorf, J. Shirck, R. M. Walker, *Proc. Lunar Planet. Sci. Conf. 9th* (1978), p. 1187.
5. Particles were selected for this study on the basis of (i) approximately chondritic ratios for major elements detected by energy-dispersing x-ray and (ii) a reentrant aggregate structure as seen in the scanning electron microscope. After selection, they were individually cleaned of the silicone oil collecting medium in a running stream of hexanes. Following the microhandling procedures described by Flynn *et al.* (4), we individually mounted and characterized them by optical microscopy, scanning electron microscopy, and energy-dispersive x-ray analyses. Finally the particles were placed individually into a "boat" of high-purity nickel foil; we used a dry glass needle, coaxial reflected illumination, and a tiny ($\sim 200 \mu\text{m}$) glass "dust pan" to minimize the chance of particle loss during transfer. The nickel foil (15 mg) was then completely folded, spot welded at the ends to form a loop, and stored in dry nitrogen prior to loading into the gas extraction system. The time that elapsed between the cleaning of the particles and completion of the mount was 3 days. Atmospheric exposure was thus minimized. In addition, after having been loaded into the vacuum system, the particles were heated to 50°C for 1 day to help remove any adsorbed atmospheric gases.
6. P. Fraundorf, thesis, Washington University (1980).
7. C. M. Hohenberg, *Rev. Sci. Instrum.*, in press.
8. T. J. Bernatowicz, C. M. Hohenberg, F. A. Podosek, *Proc. Lunar Planet. Sci. Conf. 10th* (1979), p. 1587.
9. P. Eberhardt, J. Geiss, H. Graf, N. Grögler, U. Krähenbühl, H. Schwaller, J. Schwarzmüller, A. Stettler, *Proc. Apollo 11 Lunar Sci. Conf.* (1970), p. 1037.
10. J. Zahnring, *Z. Naturforsch. Teil A* **17**, 460 (1962).
11. J. Geiss, in *13th International Conference on Cosmic Rays: Conference Papers* (Univ. of Denver Press, Denver, 1973), pp. 3375-3398.
12. C. M. Hohenberg, K. Marti, F. A. Podosek, R. C. Reedy, J. R. Shirck, *Proc. Lunar Planet. Sci. Conf. 9th* (1978), p. 2311.
13. J. H. Reynolds and G. Turner, *J. Geophys. Res.* **69**, 3263 (1964).
14. K. Marti, *Science* **166**, 1263 (1969).
15. J. Reynolds, *Phys. Rev. Lett.* **4**, 351 (1960).
16. R. S. Lewis, B. Srinivasan, E. Anders, *Science* **190**, 1251 (1975).
17. P. Harteck and R. R. Reeves, Jr., in *Encyclopedia of Atmospheric Sciences and Astrogeology*, R. W. Fairbridge, Ed. (Reinhold, New York, 1967), pp. 66-70.
18. D. L. Lind, J. Geiss, W. Stettler, *J. Geophys. Res.* **84**, 6435 (1979).
19. T. J. Bernatowicz and F. A. Podosek, in *Terrestrial Rare Gases. Advances in Earth and Planetary Sciences*, E. C. Alexander and M. Ozima, Eds. (Japan Scientific Societies Press, Tokyo, 1978), vol. 3, pp. 99-135.
20. D. E. Brownlee, in *Protostars and Planets*, T. Gehrels, Ed. (Univ. of Arizona Press, Tucson, 1978), pp. 134-150.
21. We are grateful to D. Brownlee for providing the particles for this work and for his counsel in the particle-handling techniques. We thank R. M. Walker for encouraging this work and for many stimulating discussions. Supported in part by NASA grants NAG-9-7 and NGL 26-008-065.
- * Present address: 3M Center, Building 201-3E, St. Paul, Minnesota 55133.

24 March 1980; revised 23 October 1980

Solar Cycle Signal in Earth Rotation: Nonstationary Behavior

Abstract. Following the discovery of the 11-year solar cycle signal in earth rotation, linear techniques were employed to investigate the amplitude and phase of the difference between ephemeris time and universal time (ΔT) as a function of time. The amplitude is nonstationary. This difference was related to $\Delta(\text{LOD})$, the difference between the length of day and its nominal value. The 11-year term in $\Delta(\text{LOD})$ was 0.8 millisecond at the close of the 18th century and decreased below noise level from 1840 to 1860. From 1875 to 1925, $\Delta(\text{LOD})$ was about 0.16 millisecond, and it decreased to about 0.08 millisecond by the 1950's. Except for anomalous behavior from 1797 to 1838, ΔT lags sunspot numbers by 3.0 ± 0.4 years. Since ΔT lags $\Delta(\text{LOD})$ by 2.7 years, the result is that $\Delta(\text{LOD})$ is approximately in phase with sunspot numbers.

Currie (1) examined the time discrepancy between ephemeris time and universal time, $\Delta T = ET - UT$, from 1764 to 1978 compiled from four sources (2) and discovered the 11-year solar cycle signal in the record. Two-channel maximum entropy spectrum analysis (MESA) (3, 4) between ΔT and sunspot numbers, R_z (5), over different time spans suggested that the amplitude was nonstationary in time. In order to elucidate the time domain structure of the signal, a one-channel MESA of the entire ΔT record, linear prediction error smoothing, and band-pass filtering were employed. The analysis demonstrates that the signal is nonstationary and also shows that ΔT lags R_z , except for the interval 1797 to 1838. Since most salient results are presented in the time domain, an important side benefit of the analysis is that readers inexperienced in frequency-domain signal processing can visually assess the evidence.

A high-pass, zero phase shift filter with $2N + 1$ ($N = 10$) weights, whose frequency response is shown in Fig. 1a,

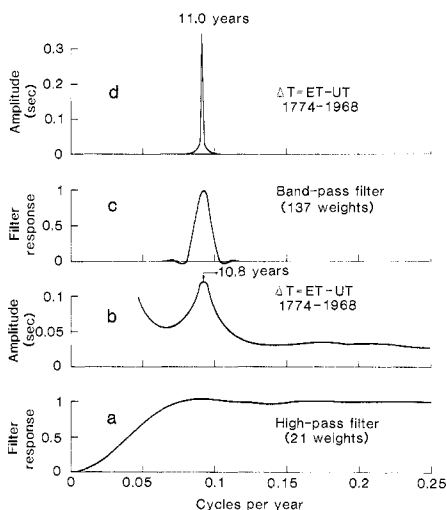


Fig. 1. (a) Frequency response of $2N + 1$ ($N = 10$) high-pass filter applied to ΔT and R_z series from 1764 to 1978. (b) Spectrum of high-pass filtered ΔT series. (c) Frequency response of $2N + 1$ ($N = 68$) band-pass filter applied to high-pass filtered extended ΔT series. (d) Spectrum of band-pass filtered ΔT series.

was convolved with the ΔT and R_z records. The response of the filter is unity for periods less than 15 years. The high-pass filtered series are plotted in Fig. 2, a and b. Fluctuations in ΔT are in the general range -2 to 2 seconds, and much of this power is ascribed (6) to hydromagnetic dynamo fluctuations in the earth's core (annual values of ΔT are given to an accuracy of 0.01 second).

Single-channel MESA (7) can be conceptually grasped by considering a common circumstance in the physical sciences. An observed input time series is passed through a "black box" that modifies the frequency and phase characteristics of the input to produce an output series. In the frequency domain the spectrum of the output series divided by that of the input equals the transfer function of the black box. In MESA the black box is termed a prediction error filter (PEF), and the filter is designed to reduce an arbitrary input series into an output random noise sequence whose spectrum is a constant. The spectrum of the input is thus proportional to a constant divided by the transfer function of the PEF.

In MESA the resolution of a sinusoidal signal is quite sensitive to the signal-to-noise ratio (SNR) and the length of the time series relative to the period of the sinusoid. As the SNR decreases the length (the order or the number of weights in the filter) of the PEF must be increased; as the record length decreases the PEF must also be increased (8). Single-channel MESA was applied to the ΔT series in Fig. 2a for increasing order of the PEF. The 11-year term became well resolved for a PEF of order 15, and the spectrum is depicted in Fig. 1b. For a longer PEF the peak bifurcates. Cohen and Lintz (9) suggested that the nominal 11-year term in the R_z record consists of several discrete frequency components. Such a model is not tenable for ΔT because objections (10) to a discrete multi-frequency Chandler wobble apply equally to the 11-year term in earth rotation (11).

The next task was to design a band-pass filter centered at 10.8 years whose